BEHAVIOUR OF RC SPANDREL BEAM IN EXTERIOR WIDE BEAM-COLUMN CONNECTIONS

H. Behnam[(1)], J.S. Kuang[(2)], K. Abdouka[(3)]

[(1)] PhD Candidate, Hong Kong University of Science and Technology, Hong Kong. hbehnam@connect.ust.hk
[(2)] Professor, Hong Kong University of Science and Technology, Hong Kong. cejkuang@ust.hk
[(3)] Senior Lecturer, Swinburne University of Technology, Melbourne, Australia. kabdouka@swin.edu.au

Abstract

According to architectural and structural needs, heavily loaded and long span moment frames are often built with the beams wider than the framing column. Wide beam-column connections in this structural typology play a significant role in determining the overall seismic behaviour of the structures. This paper presents the results of a set of experiments performed on two full-scale exterior wide beam-column connections. The specimens have the same dimensions and reinforcement detailing, except for the reinforcement detail in spandrel beam. The control specimen had both longitudinal and transverse reinforcement within the spandrel beam while the other specimen had no reinforcement in the spandrel beam. According to the results of the test, the failure mode in the control specimen was ductile with beam flexural hinging followed by joint and spandrel beam torsional failure, while it changed to the brittle torsional failure of spandrel beam in the other specimen. The specimen with no reinforcement in its spandrel beam exhibited brittle torsional failure with an average reduction of 37% in the wide beam flexural strength capacity compared to the control specimen. In addition to the experimental study, nonlinear three-dimensional finite element analysis was conducted to model the behaviour of tested specimens using monotonic loading analysis and to investigate the load transfer mechanism in wide beam-column connection. The results from both experimental and numerical investigation indicated that the level of joint shear stresses and the level of spandrel beam torsional stresses should be controlled to achieve an acceptable and adequate seismic performance.

Keywords: *wide beam-column connection; full-scale test; spandrel beam; finite element analysis; joint shear stresses; torsional stresses.*

Introduction

In the areas of moderate to low seismicity, such as Australia, Hong Kong, and the majority of European countries, reinforced concrete moment resisting frames with wide beam-column connections have been used extensively. This structural system offers a medium storey height as well as lateral stiffness compared to reinforced concrete conventional frames and flat-slab structures. In comparison with conventional frames, it offers lower floor-to-floor height, less congested joint region, simplified formwork, and fast construction at a

reduced cost. Compared to flat-slab structures, it affords longer spans and more freedom on the column grid arrangements (LaFave and Wight 1999; Benavent-Climent 2007; Li and Kulkarni 2009; Elsouri and Harajli 2015; Davey et al. 2013). Because of these advantages, there is an increasing trend in adopting this structural system even in the regions of high seismicity.

A literature review on the wide beam-column connections behaviour can reveal two important features. First, exterior wide beam-column connections are not only susceptible to joint shear failure but also, they are extremely vulnerable to torsional failure of the spandrel beam. Second, the torsional behaviour of transverse beams strongly influences the overall seismic behaviour of wide beam-column connections. (LaFave and Wight 2001; Benavent-Climent 2009 and 2010; Goldsworthy, and Abdouka 2012; Siah et al., 2003; Stehle et al., 2001).

Despite these facts, the new wide beam frame buildings are designed and constructed around the world, with no particular consideration given to the torsional behaviour of the spandrel beams. Furthermore, the majority of existing wide beam frame buildings were designed and built when the relevant code of practice had no seismic design provisions. The severe damage and collapse of these buildings in the recent earthquakes are the results of Inadequate reinforcement detailing. Most of the existing wide beam-column frame building share the following shortcomings: (1) absence of transverse reinforcement in the joint region; (2) insufficient bond length of the beam bars; (3) lack of torsional reinforcement in the spandrel beam to sustain torsion; and (4) substantially wide beam which exceeds the limits prescribed by the current seismic codes (Benavent-Climent 2007; Fardis 2009; Lopez-Almansa et al. 2013; Dominguez et al. 2016). Therefore, analysis, design, and detailing of the exterior wide beam-column connections are critical issues that need to be carefully addressed.

The existing test database on exterior wide beam-column connection is very limited, and it cannot address all behavioural aspects of the wide beam-column connections. Therefore, modelling is necessary. Nonlinear three-dimensional finite element model (FEM) is capable of accurately modelling the mechanical properties, crack formation and propagation, deflections, and possible failure mechanisms in reinforced concrete members. However, considering the popularity of FEM, relatively few studies have been reported to date of applying FEM to wide beam-column connections (Li and Kulkarni 2009 and 2010). The most challenging aspect is how to accurately modelling the concrete in tension and compression and reinforcing bars in the model. In the past, different theories and formulations for constitutive modelling of concrete have been developed and implemented in FEM computer softwares. Among the constitutive models for simulating the behaviour of concrete, the concrete damaged plasticity (CDP) model has proved to provide the most stable regime. The CDP has the ability to capture the post-peak behaviour with reliable accuracy when compared to the experimental results (Jankowiak and Lodygowski 2005; Birtel and Mark 2006; Mohamed 2014; Genikomsou and Polak 2015; Wosatko et al. 2015;).

The objective of this study is to explore the influence of the spandrel beam on the performance of the exterior wide beam-column connection. Two full-scale exterior wide beam-column connections were tested to determine the overall seismic performance of the connections and to evaluate the important aspects of their responses quantitatively. The tests are an extension of our previous research on the seismic performance of wide beam-column connections, which was part of a program for earthquake resistance structures. Furthermore, nonlinear three-dimensional FEM was conducted to study the load transfer mechanism within the connection region. The CDP, which is offered in Abaqus (Abaqus 2013) was adopted for the representation of concrete. The numerical results are compared to the test results regarding deflections, strength and crack patterns.

Experimental program

The experimental program aims at investigating the influence of the spandrel beam on the seismic behaviour of wide beam-column connections. Figs. 1 and 2 show the geometry and reinforcing details of the tested specimens, designated as S4, and S5. The specimens representing a portion of the framing system are obtained by terminating the beam at its mid-span and the columns at their mid-heights, where inflection points are likely to occur under the lateral loads. Due to the laboratory limitation, the beam span in the frame was only considered to be 3 meters. Testing beam-column specimens with the shorter beam is a common practice in this field (Elsouri and Harajli 2015; Kotsovou and Mouzakis). Specimens have an identical beam length of 1500 mm with a cross-section of 750 mm × 300 mm and the same column height of 3100 mm with a cross-section of 300 mm × 360 mm. The columns were reinforced with bars of 16 mm diameter (10D16), amounting to a 1.85% column reinforcement ratio. Specimen S4 contained a shallow depth spandrel beam with a cross-section of 360 mm × 300 mm. The spandrel beam in this specimen consisted of 8D16 longitudinal bars and having D10 closed stirrup at 70 mm distance (Fig. 1). In the specimen S5, there was no reinforcement in the spandrel beam. The widths of the beam in both specimens were less than the limit set by the current ACI Code (ACI 318-14:2014, $b_b < b_c + 1.5h_c$) but exceeds the limit that established by New Zealand code (NZS3101:2006, $b_b < b_c + 0.5h_c$). The column stirrups were continued through the joint. In both specimens, three layers of closed stirrups were located between beam top and bottom reinforcement in beam-column joint. Each layer consisted of four legs of a steel bar with a diameter of 10 mm. Column cross-section and reinforcement detail are shown in Figs. 1 and 2.

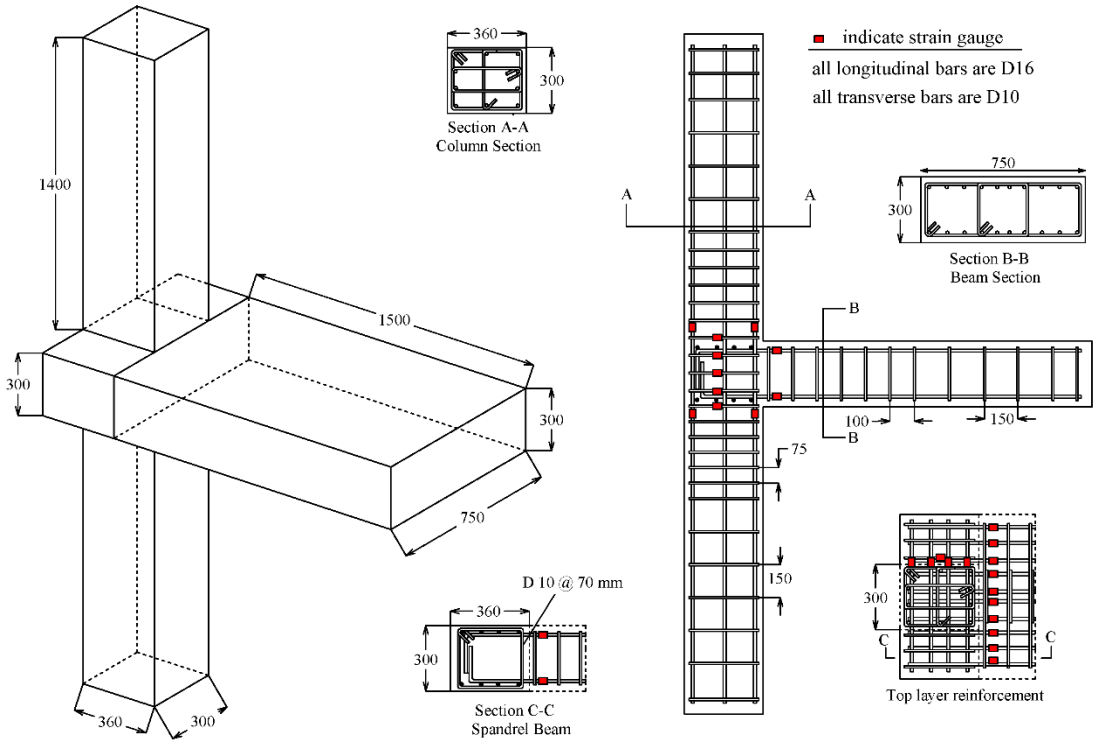

Fig. 1. Dimensions and reinforcement details of specimen S4 (unit: mm).

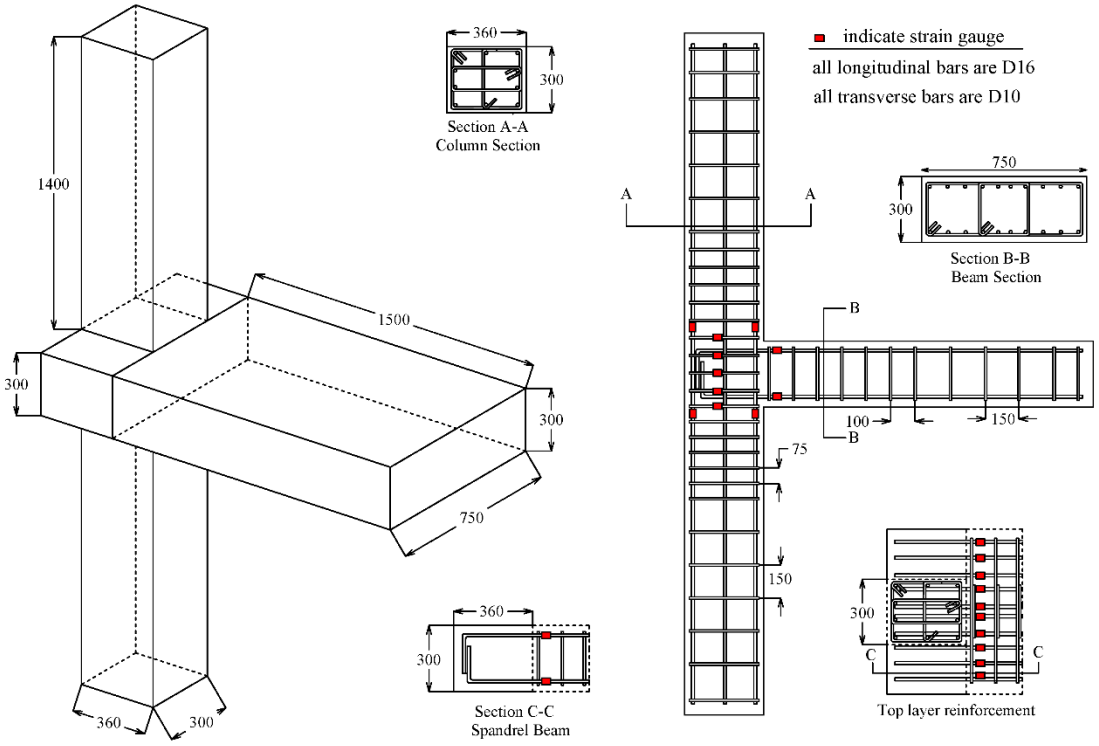

Fig. 2. Dimensions and reinforcement details of specimen S5 (unit: mm).

Expected capacities

The concrete compressive strength on the test day was 34.7 MPa and 34.2 MPa, in specimens S4 and S5, respectively. The average yield stress of the longitudinal reinforcement (D 16 mm) and stirrup (D 10 mm) were 558 MPa and 511 MPa. The main design parameters of the specimens such as the column ($M_{n,c}$) and beam ($M_{n,b}$) nominal flexural capacities, column-to-beam flexural strength ratio (M_r), estimated lateral load ($V_{b,e}$), factored torsion applied to spandrel beam (T_u), nominal torsional moment strength (T_n), joint shear demand ($V_{j,e}$), and joint shear capacity (V_n) were estimated based on the measured properties of materials and ACI 318-14 criteria. The specimen capacities were calculated using the actual material strength and they are referred to as expected strengths, as summarised in Table 1.

Table 1 shows the minimum column-to-beam flexural strength ratio (M_r) was 1.53, which satisfies the "strong column-weak beam" philosophy. The factored torsional moment on the side face of the column, T_u, was estimated by multiplying the overstrength factor of 1.25 by the applied torsional moment. The ratios of T_u/T_n in specimens S4, and S5 were 1.56, and 6.63, respectively. ACI 352R-02 requires these ratios to be lower than one. Therefore, torsional failure of the spandrel beam was expected in both specimens. In specimen S5, there was no reinforcement in the spandrel beam and the torsional capacity was taken as the concrete cracking torque.

Table 1. Main design parameters and expected capacities.

Specimen	$M_{n,c}$ kNm	$M_{n,b}$ kNm	M_r[a]	$V_{b,e}$[b] kN	T_u kNm	T_u/T_n[c]	$V_{j,e}$[d] kN	γ_e[e]	γ_{ACI}
S4	187	243.8	1.53	184.7	114	1.56	1292	2.03	1.25
S5	187	243.3	1.54	184.3	114	6.63[f]	1293	2.05	1

[a] $M_r = \sum M_{n,c} / \sum M_{n,b} \geq 1.2$

[b] $V_{b,e} = M_{n,b} / 1.32$

[c] $T_n = 2A_o A_t f_{yt} \cot\theta / s$, where A_o= 0.85A_{oh}=*0.85*$x_1 y_1$, θ =45°, and s is the spacing of stirrup in the spandrel beam (s = 70mm).

[d] $V_{j,e} = 1.25A_s f_y - V_{col}$, where A_s is the beam flexural reinforcement area and V_{col} is the column shear force.

[e] $\gamma_e = V_{j,e} / V_n = V_{j,e} / \left(\sqrt{f_c} b_c h_c \right)$

[f] $T_n = T_{cr} = 0.33 \sqrt{f_c} A_{cp}^2 / P_{cp}$

Table 1 also shows that the expected normalised joint shear stress ratio (γ_e) was larger than the ACI requirement. The γ_e should be smaller than 1.25, and 1.0 for specimens S4, and S5, respectively. The ACI code only considers the column cross-sectional area ($b_c \times h_c$) to resist joint shear stresses. Since the joint shear force was greater than the joint shear capacity, joint shear failure was expected in all specimens.

Test setup, loading sequence, instrumentation, and measurements

The schematic test setup is shown in Fig. 3. The test setup was arranged on the test floor, and for the convenience of applying loading and testing, each beam-column assembly was rotated 90° from the true orientation (column positioned horizontally and beam positioned vertically). The beam tip was linked to an actuator with a swivel connector to apply the lateral load. Initially, an axial load of 480 kN (12.8% of the column axial capacity) was applied to the column through a hydraulic jack. The axial force was applied in a force controlled mode and was maintained constant through the test. Then, the lateral cyclic displacement (Δ) was applied to the top of the beam in two opposite directions. The lateral load history consisted of several sets of three cycles with different horizontal displacements amplitudes, as shown in Fig 4. The drift ratio (%) is expressed as the ratio of the applied displacement to the beam length plus half of the column depth. The same loading history and test setup were used for both specimens. The similar test setup was adopted in previous research to study the behaviour of both gravity designed specimens and moment resistance connections (Hung and Jen 2007, Wong and Kuang 2008, among them). Effect of gravity induced moment on the beam is important but by using aforementioned test setup gravity moment is not being incorporated in the test. Since the ultimate capacity of the connection and comparative behaviour of two specimens was the main objective of this paper, ignoring the gravity induced moment on the beam is acceptable.

Specimens were instrumented extensively by fixing strain gauges at critical locations identified on the reinforcement bars to record the magnitude of the reinforcement strains that were developed at different loading stages. The locations of the strain gauges on the longitudinal and transverse steel bars in the beam and column are shown in Figs. 2 to 5, as red colour spots. Linear variable displacement transducers (LVDTs) were used to measure the displacement at various locations on the specimen as shown in Fig. 3.

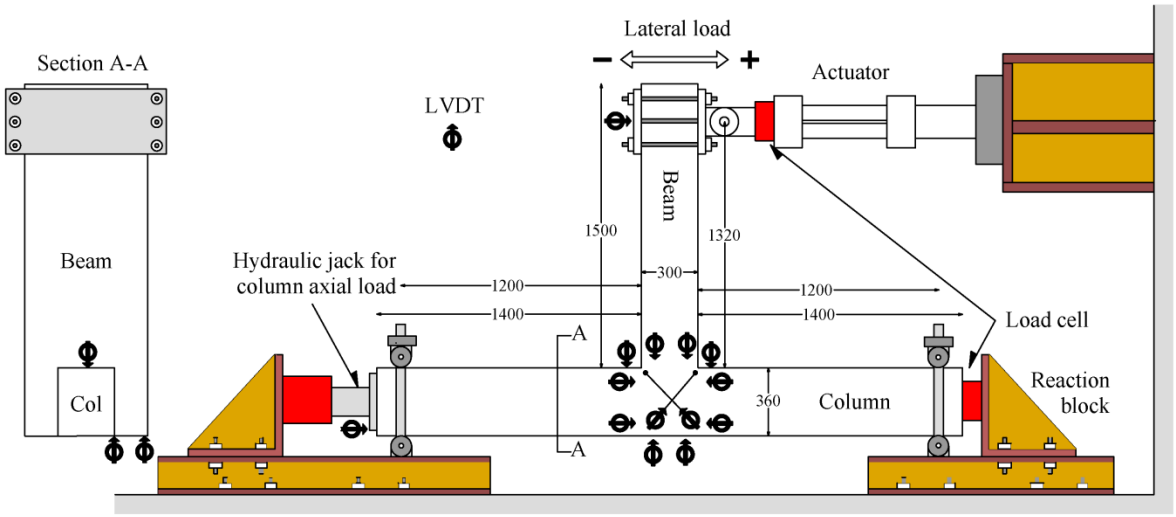

Fig. 3. Schematic view of the test setup (unit: mm).

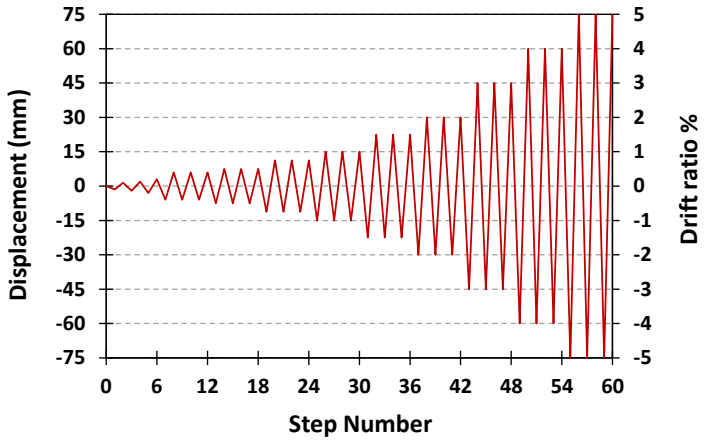

Fig. 4. Cyclic displacement history.

Experimental results and observations

The final failure patterns of the specimens were obtained from repeated reverse cyclic loading, as shown in Fig 5. In the specimen S4, first flexural cracks were formed across the full width of the beam at a 0.2% drift ratio. In the drift ratio of 1.5%, flexural cracks continued to develop into full width of the beam near the beam-column interface. At a drift ratio between 2% and 3%, the diagonal shear cracks on the joint tended to widen, indicating the start of the joint shear failure. Torsional cracks were appeared in the spandrel beams starting at a drift ratio of 0.75%. These inclined torsional cracks developed around the spandrel beam and

extended to the intersection region of the column sides and beam at a drift ratio of 3%. The joint shear and torsional failure of spandrel beam after beam yielding were evident due to the wide-opened diagonal shear cracks, and the visible expansion of concrete from the joint and the spandrel beam region. In specimen S5, the first hairline flexural crack was developed in the joint interface section at a drift ratio of 0.2%. At a 1% drift ratio, the torsional cracks developed rapidly, wrapping around the spandrel beams diagonally. At 2% drift ratio, the spandrel beam was completely separated from the column face and a complete loss in the torsion capacity of the spandrel beams occurred, which triggered a considerable reduction in the lateral load capacity. In the subsequent cycles, the separated spandrel beam started to slide along the shear planes near the column faces. The crack pattern at the end of the test was characterised by severe torsion cracking in the spandrel beam near the column face and minor flexural cracks at the beam.

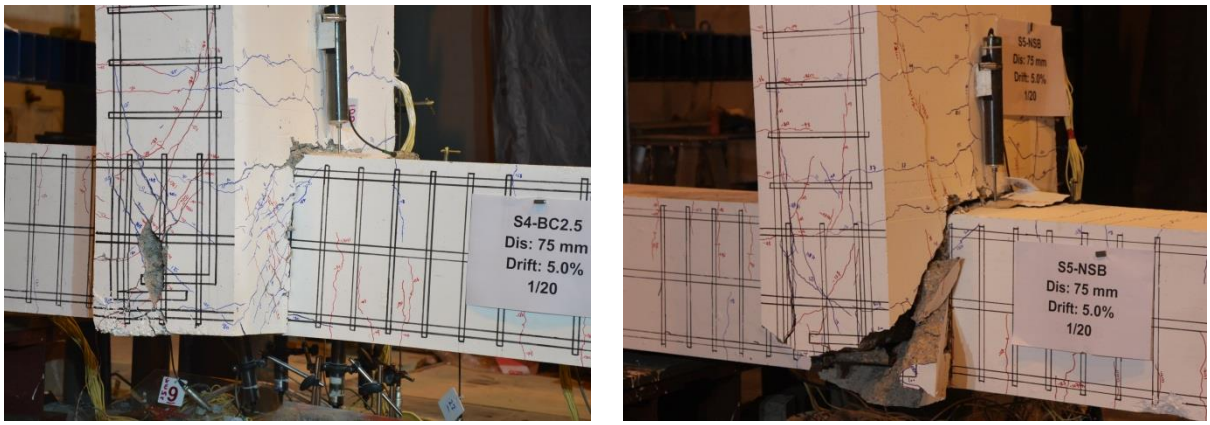

(a) Specimen S4 (b) Specimen S5

Fig 5. crack pattern at 5% drift ratio (end of test)

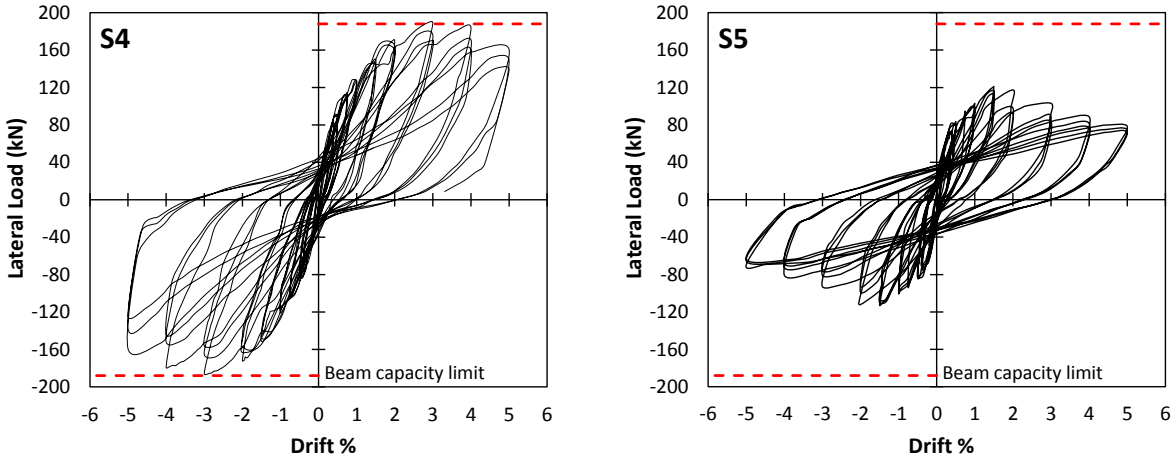

(a) Specimen S4 (b) Specimen S5

Fig. 6. Lateral load-drift hysteretic response.

Fig 6 illustrates the lateral load versus the drift ratio of the specimens in the form of hysteresis curves. Specimen S4 reached its theoretical capacity at a drift ratio of 3% in both loading directions. Then, its strength degraded until the end of the test. The hysteresis loops of this specimen showed considerable pinching, which was primarily attributed to the formation of diagonal shear and torsion cracking in the joint and spandrel beam. Specimen S5 experienced significant strength loss compared to the specimen S4 due to the torsional failure of the spandrel beam. This specimen did not reach its theoretical capacity, while it attained the maximum capacities of -114.5 kN and 120.8 kN which are approximately 62% and 65% of the theoretical strength. The strength of this specimen decreased significantly from the following loading cycles until the end of the test. As shown in Fig. 6(b), there is a certain level of lateral force transfer that appears to be maintained up to the 5% drift ratio. The residual load-carrying capacities in this specimen were -69.4 kN and 78.4 kN, which are 38% and 42% of the theoretical capacities. This load level is consistent with the moment transferred directly from the central part of the beam to the column.

The test results showed that the behaviour of the spandrel beam strongly affects the overall load-displacement relationship, crack pattern, joint shear capacity and failure mode of the specimens. The maximum torsion applied to the spandrel beam was determined by measuring the strain in the beam longitudinal reinforcement, which was 84, and 39.7 kNm in the specimens S4, and S5, respectively. The ratio of the maximum applied torsion to the spandrel beam torsional capacity was 1.15, and 2.30, respectively. In the specimen S5, the maximum torsion was 57% larger than the spandrel beam cracking torque capacity, and the specimen failed in torsion. In the specimen S4, the actual torsion acting on the spandrel beam was almost 15% larger than the spandrel beam capacity. However, it exhibited a very severe torsion cracking and concrete crushing in the spandrel beam. The crushing of the concrete occurred because basically, the cross section of the spandrel beam was not enough to resist applied torsion. According to the ACI 352R-02, in the exterior wide beam-column connections, the spandrel beam should be designed for full equilibrium torsion from the beam and slab bars. However, before determining the required transverse and longitudinal reinforcement for the torsion the adequacy of the cross-section for torsion must be checked. Cross-sectional dimensions are limited to help reduce the unsightly cracking and to prevent crushing of the inclined concrete compression struts due to the shear and torsion.

Finite element simulations

To further enhance the understanding of the complicated behaviour of the wide beam-column connections, a nonlinear finite element analysis was carried out. In the numerical study, the geometrical properties of the model were kept similar to the test specimens. Eight-noded hexahedral (brick) elements (C3D8R) were used for concrete with reduced integration to avoid the shear locking effect. Two-noded linear truss elements (T3D2) were used to model reinforcements. The embedded method was adopted to simulate the bond between the concrete and the reinforcement which was assumed perfect. After carrying out mesh sensitivity study, the mesh size of 30 mm was adopted in all models. Analogous to the test condition, a loading was defined in two steps. First, the column axial load was applied up to the required level. In the second phase, a lateral displacement was applied in the beam end. Static analysis in Abaqus/Standard with viscosity regularisation was performed.

Material models

Concrete Damaged Plasticity (CDP) model (Lubliner et al. 1989; Lee and Fenves 1998) is used as the constitutive model for concrete material. The concrete material parameters used as input variables in the CPD model are the density, modulus of elasticity E_c, Poisson's ratio ν, compressive and tensile strengths of the concrete and damage parameter in compression and tension. The concrete behaviour in tension is characterised by a stress-crack displacement response, as shown in Fig. 7, where f_t is the maximum tensile strength and G_f denotes the fracture energy of concrete that represents the area under the tensile stress-crack displacement curve. Adopting stress-crack width displacement based on the fracture energy can prevent mesh-sensitivity and allow for numerical convergence. The fracture energy of concrete G_f (N/m) for ordinary normal weight concrete can be obtained from CEB-FIP Model Code 2010.

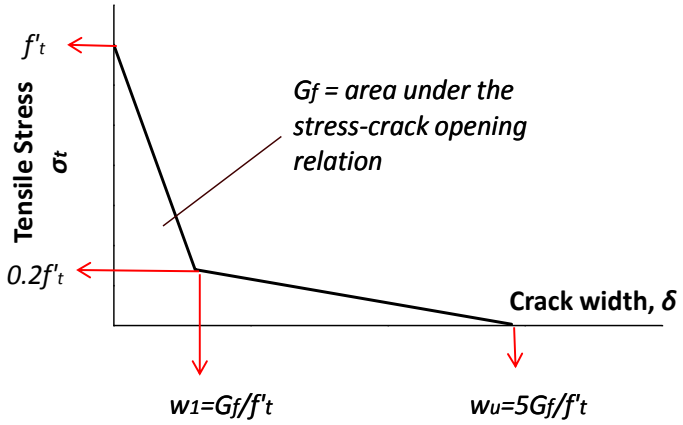

Fig. 7. Uniaxial tensile stress-crack width relationship for concrete.

The concrete stress-strain behaviour under compressive loading was modelled in three phases (Fig. 8). Equations for the assumed compressive stress-strain diagram were suggested by (Birtel 2006) and are given in Eqs. (1a, b, and c) by slight modifications.

$$\sigma_{c(1)} = E_c \varepsilon_c, \quad \varepsilon_c \le 0.4 f_c / E_c \tag{1a}$$

$$\sigma_{c(2)} = \frac{\eta_c \frac{\varepsilon_c}{\varepsilon_0} - \left(\frac{\varepsilon_c}{\varepsilon_0}\right)^2}{1 + (\eta_c - 2)\frac{\varepsilon_c}{\varepsilon_0}} f_c, \quad 0.4 f_c / E_c \le \varepsilon_c \le 0.0035 \tag{1b}$$

$$\sigma_{c(3)} = \left(\frac{2 + \lambda f_c \varepsilon_0}{2 f_c} - \lambda \varepsilon_c + \frac{\lambda \varepsilon_c^2}{2 \varepsilon_0} \right)^{-1}, \quad 0.0035 \le \varepsilon_c \le \varepsilon_u \tag{1c}$$

Eq. (1a) represents the linear-elastic branch in which ε_c is a variable changing from zero to $0.4f_c/E_c$, and E_c is the initial modulus of elasticity. The linear branch ends at the stress level of $0.4f_c$. Eq. (1b) describes the ascending branch up to the strain level of 0.0035. The corresponding strain level at the peak stress is defined as $\varepsilon_0 = 2f_c/E_c$; η_c is the material constant. The stress and strain compatibility at the strain level of $\varepsilon_c = 0.4f_c/E_c$, for Eq. (1a) and (1b) gives the value of η_c. Eq. (1c) shows the third and descending branch; λ is the constant crushing energy as a material property. Using the stress and strain compatibility at the strain level of ε_c = 0.0035, for Eq. (1b) and (1c) enables the value of λ to be determined. Damage parameters were introduced in the CPD model in tension and compression according to Figs. 9 and 10, respectively (Genikomsou and Polak (2015)). The uniaxial stress-strain relation of the reinforcement is modelled as elastic with Young's modulus (E_s) and Poisson's ratio (v) having typical values of 200,000 MPa and 0.3, respectively. Table 2 summarises the main concrete parameters used in the model.

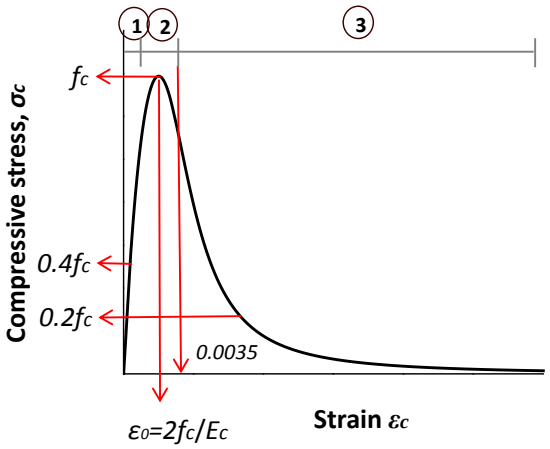

Fig. 8. Uniaxial compressive stress-strain relationship for concrete.

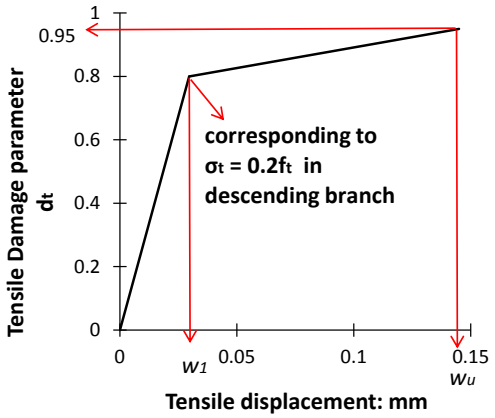

Fig. 9. Tensile damage parameter-strain relationship for concrete.

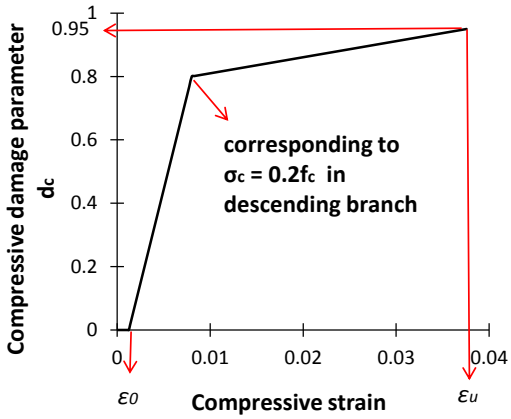

Fig. 10. Compressive damage parameter-strain relationship for concrete (simplified in linear form).

Table 2. Properties of concrete.

Specimen	f_c MPa	E_c[a] MPa	ε_0[b]	f_t[c] MPa	G_f N/mm	Poisson's Ratio (v)	Density tonne/mm^3
S4	34.7	27700	0.00251	2.8	0.083	0.2	2.4E-009
S5	34.2	27500	0.00248	2.8	0.083	0.2	2.4E-009

[a] $E_c = 4700\sqrt{f_c(MPa)}$, Module of elasticity

[b] $\varepsilon_0 = 2 f_c / E_c$,

[c] measured using four-point loading tests on test day.

In addition to defining the material parameters, the following data were also provided.

- σ_{b0}/σ_{c0} is the ratio of biaxial compressive to uniaxial compressive yield stress, set to 1.16;
- K_c is the coefficient determining the shape of the deviatoric cross-section, configured toa value of 0.667;
- ψ is the dilatation angle, physically interpreted as the internal friction angle of concrete, taken as 40;
- ε is the potential flow eccentricity, assumed with a default value of 0.1; and
- μ is the viscosity parameter used for the viscoplastic regularisation of the concrete constitutive equations in the Abaqus/Standard analyses, taken as 0.00001.

Comparison of FEA predictions with experimental results

Fig. 11 presents the analysis results together with the experimental hysteretic loops in terms of load-displacement. As illustrated in this figure, the lateral force-displacement curve predicted by the FEA follows most of the experimental curve closely. Both results show similar post-peak softening behaviour.

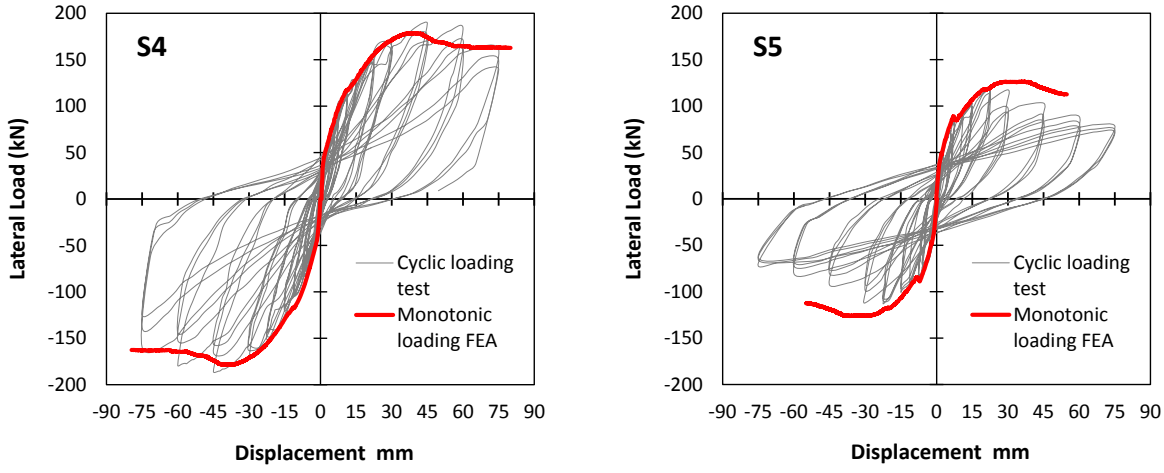

(a) Specimen S4 (b) Specimen S5

Fig. 11. Load-displacement from experiment and numerical analysis.

Fig. 12 shows the cracking pattern on the tension side of the beam at 5% drift, from the FEA. The obtained FEA crack patterns were similar to the cracks that observed during the test and shown in Fig 5. The simulated response of the test specimens was in good agreement with the results found from the experiment. The modelled responses verified the ability of the selected material parameters and constitutive models to capture the behaviour of the connections up to the end of the tests. The ratio of the predicted maximum lateral force in the beam to that of the test results was within an error of ± 9%. The presented analyses indicate that the proposed model can simulate the nonlinear behaviour of RC wide beam-column connections, and it can be used for parametric studies on various aspects influencing the behaviour of wide beam-column connections.

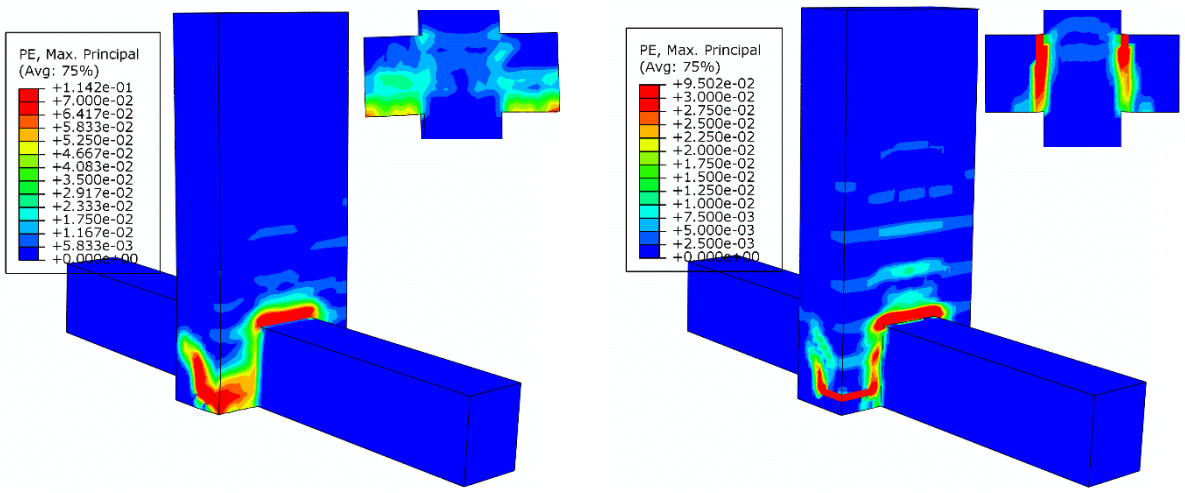

(a) Specimen S4 (b) Specimen S5

Fig. 12. Cracking pattern on tension surface at 5% drift

In addition to the crack pattern, the stress distribution in tension reinforcement was compared. Beam bar yielding for the beam top reinforcement anchored inside the column core occurred in the 1.67%, and 1.5% drift cycles in the specimens S4, and S5, respectively. Beam bars anchored outside the column core of the specimen S5 never yielded. The entire beam bar yielded at a 2.5% drift ratio in specimens S4. In the specimens S4 joint shear failure and spandrel beam, torsional failure occurred at a drift ratio of 3%. Specimen S5 failed in a brittle torsional mode. The FEA showed a same yielding pattern as the reinforcement.

Figs. 13 and 14 represents the concrete compressive stress trajectories for tested specimens. Fig 13a and 14a clearly show that the primary load transfer mechanism through and around the joint is the diagonal strut mechanism. Fig 13b shows the stress distribution of the portion of wide beam outside the column width is non-uniform. Part of the loading in this region is transferred to the beam-column joint directly through the diagonal paths. The remaining portion of loading passes towards the transverse beams first and then transfers to the joint core through torsion. The concrete compressive struts cannot develop in outside portion of the beam in specimen S5, because of the lack of the spandrel beam reinforcement.

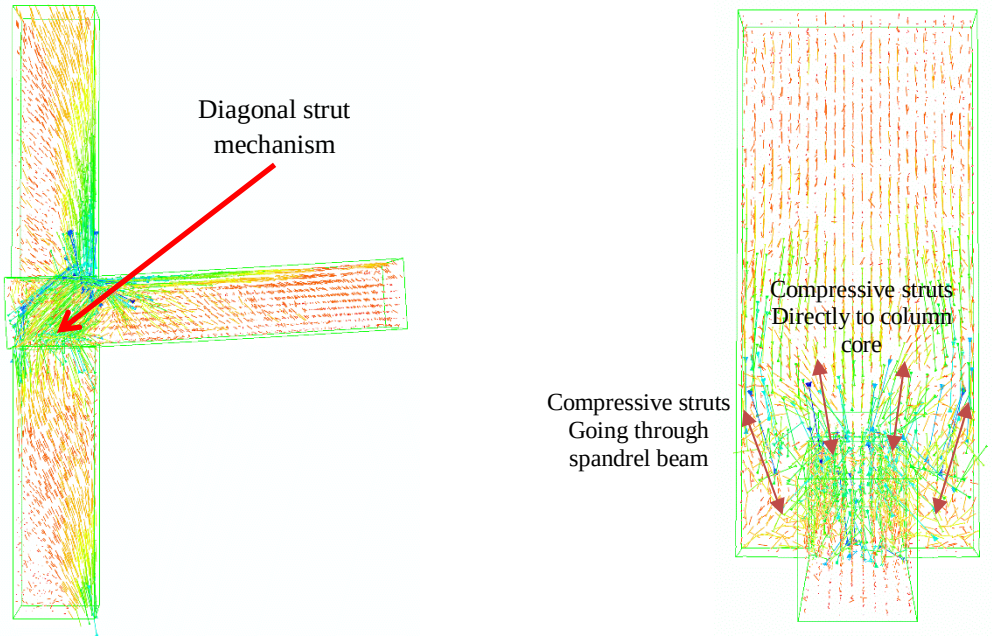

(a) Side view (b) Top view

Figure 13. Load transfer paths in concrete in specimen S4

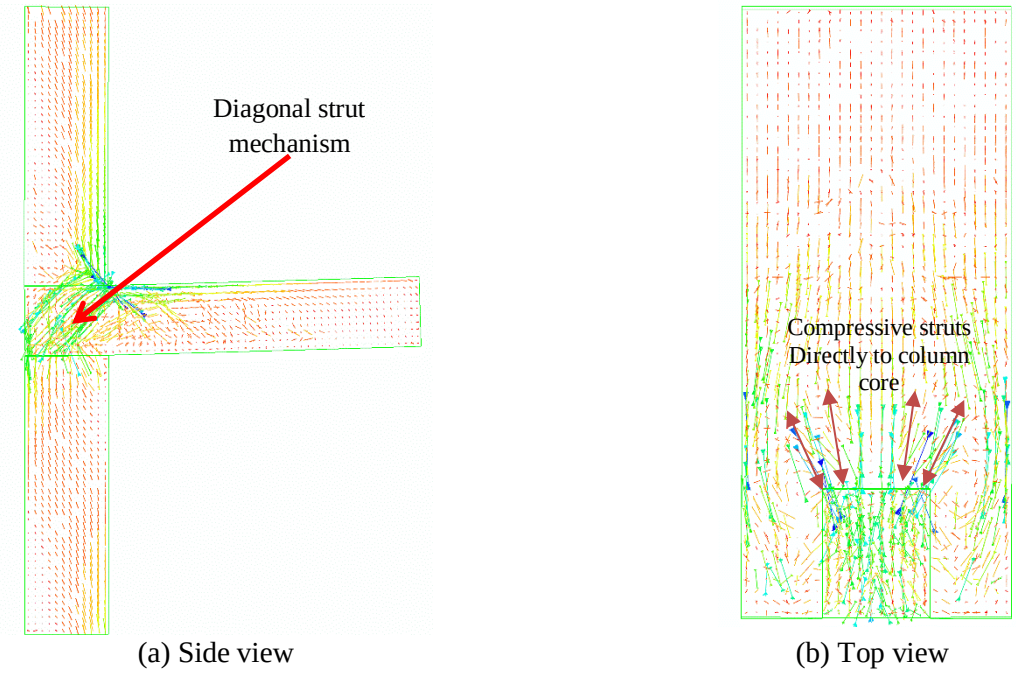

(a) Side view (b) Top view

Figure 14. Load transfer paths in concrete in specimen S4

From the observed performance of the specimens and also from the results of the numerical modelling, it can be concluded that the spandrel beam has a vital effect on the seismic behaviour of the exterior wide beam-column connections. Providing both longitudinal and transverse reinforcements in spandrel beam is necessary to resist torsion and to develop adequate concrete struts. According to the results of the test and numerical analysis, it is suggested that spandrel beam should be designed for full equilibrium torsion. However, before determining the required transverse and longitudinal reinforcement for the torsion the adequacy of the cross-section for torsion must be checked. Cross-sectional dimensions are limited to help reduce the unsightly cracking and to prevent crushing of the inclined concrete compression struts due to the shear and torsion

Conclusions

An experimental and numerical investigation of two full-scale exterior reinforced concrete wide beam-column connections was carried out to study the influence of the spandrel beam on the overall behaviour of wide beam-column connections. The spandrel beam in specimen S4 included both longitudinal and transverse reinforcements, but there was no reinforcement within the spandrel beam of the specimen S5. The following conclusions can be drawn.

1- Beam bar yielding for the beam top reinforcement anchored inside the column core occurred in the 1.67%, and 1.5% drift cycles in the specimens S4, and S5, respectively. Beam bars anchored outside the column core of the specimen S5 never yielded due to the torsional failure of spandrel beam. The entire beam bar yielded at a 2.5% drift ratio in specimens S4.
2- The failure mode of the specimens S4 was beam flexural hinging followed by joint shear and spandrel beam torsional failure. However, specimen S5 without reinforcement in its spandrel beam failed in a brittle torsional mode with an average strength loss of 37%.
3- The ratio of the predicted maximum lateral force in the beam to that of the test results was within an error of ± 9%. The presented analyses indicate that the proposed model can simulate the nonlinear behaviour of wide beam-column connections.
4- The numerical analysis clearly showed that the primary load transfer mechanism through and around the joint is the diagonal strut mechanism. Therefore, the joint region should be confined by stirrups (similar to the conventional joints).
5- The presence of the spandrel beam's reinforcement altered the orientations of concrete diagonal struts in the spandrel beams.
6- According to the results of the test and numerical analysis, providing both longitudinal and transverse reinforcement within the spandrel beam is necessary to achieve adequate seismic performance. Therefore, it is suggested to design the spandrel beam for full equilibrium torsion. However, before determining the required transverse and longitudinal reinforcement for the torsion the adequacy of the cross-section for torsion must be checked.

Acknowledgments

The support of the Hong Kong Research Grants Council (HKRGC) under Grant Number 16209115 is gratefully acknowledged.

References

ABAQUS. Analysis user's manual 6.10. (2013), Dassault Systems Simulia Corp. SIMULIA, Providence, IR.

American Concrete Institute (ACI) Committee. (2014). "Building code requirements for structural concrete (ACI 318-14) and commentary." ACI 318-14, Farmington Hills, MI.

American Concrete Institute (ACI)-ASCE Committee. (2002). "Recommendations for design of beam-column joints in monolithic reinforced concrete structures." ACI 352R-02, Farmington Hills, MI.

Benavent-Climent, A. (2007). "Seismic behaviour of RC wide beam-column connections under dynamic loading." *J. Earthquake Eng.*, 11(4), 493-511.

Benavent-Climent, A., Cahis, X., Zahran, R. (2009). "Exterior wide beam-column connections in existing RC frames subjected to lateral earthquake loads." *Eng. Struct.*, 31(7), 1414-1424.

Benavent-Climent, A., Cahis, X., Vico, J. (2010). "Interior wide beam-column connections in existing RC frames subjected to lateral earthquake loading." *Bulletin of Earthquake Engineering*, 8(2), 401-420.

Birtel V, Mark P. (2006). "Parameterised finite element modelling of RC beam shear failure,":95-108.

CEB-FIP Model. (1990). "CEB-FIB Model Code 1990: Design code." *Bulletin d'Information* 195, London: Thomas Telford.

Davey, M., Abdouka, K., Al-Mahaidi, R. (2013). "Post-tensioned band beams as moment resisting frames under earthquake loading: a state-of-the-art review." *Aust. J. of Struct. Eng.*, 14(3), 193-205.

Dominguez, D., Lopez-Almansa, F., Benavent-Climent, A. (2016). "Would RC wide-beam buildings in Spain have survived Lorca earthquake (11-05-2011)?" *Eng. Struct.*, 108, 134-154.

Elsouri, A., and Harajli, M. (2015). "Interior RC wide beam-narrow column joints: potential for improving seismic resistance." *Eng. Struct.*, 99, 42-55.

Fardis, M. N. (2009). *Seismic Design, Assessment and Retrofitting of Concrete Buildings: Based on EN-Eurocode 8*, Springer, London.

Genikomsou AS, Polak MA. (2015). "Finite element analysis of punching shear of concrete slabs using damaged plasticity model in ABAQUS." *Eng Struct*, 98:38-48.

Goldsworthy, H. M., and Abdouka, K. (2012). "Displacement-based assessment of non-ductile exterior wide band beam-column connections." *J. Earthquake Eng.*, 16(1), 61-82.

Hung-Jen, L., & Jen-Wen, K. (2007). "Eccentric reinforced concrete beam-column connections subjected to cyclic loading in principal directions." *ACI structural journal*, *104*(4), 459.

Jankowiak T, Lodygowski T. (2005). "Identification of parameters of concrete damage plasticity constitutive model." *Foundations of civil and environmental engineering.*, 6:53-69.

Kotsovou, G., and Mouzakis, H. (2012). "Exterior RC beam–column joints: new design approach." *Eng. Structures*, 41, 307-319.

LaFave, J. M., and Wight, J. K. (2001). "Reinforced concrete wide-beam construction vs. conventional construction: resistance to lateral earthquake loads." *Earthquake Spectra*, 17(3), 479-505.

LaFave, J. M., and Wight, J. K. (1999). "Reinforced concrete exterior wide beam-column-slab connections subjected to lateral earthquake loading." *ACI Struct. J.*, 96(4), 577-585

Lee J. and Fenves G.L. (1998). "Plastic-damage model for cyclic loading of concrete structures". *Journal of Engineering Mechanics*, 124:8, 892–900.

Li, B., and Kulkarni, S. A. (2009). "Seismic behaviour of reinforced concrete exterior wide beam-column joints." *J. Struct. Eng.,* 136(1), 26-36.

Lopez-Almansa, F., Dominguez, D., Benavent-Climent, A. (2013). "Vulnerability analysis of RC buildings with wide beams located in moderate seismicity regions." *Eng. Struct.,* 46, 687-702.

Lubliner J., Oliver J., Oller S. and Onate E. (1989). "A plastic-damage model for concrete". *International Journal of Solids and Structures*, 25:3, 229-326.

Mohamed AR, Shoukry MS, Saeed JM., (2014). "Prediction of the behavior of reinforced concrete deep beams with web openings using the finite element method." *Alexandria Eng Journal*, 53:329-39.

Siah, W., Stehle, J., Mendis, P., Goldsworthy, H. (2003). "Interior wide beam connections subjected to lateral earthquake loading." *Eng. Struct.,* 25(3), 281-291.

Stehle, J. S., Goldsworthy, H., Mendis, P. (2001). "Reinforced concrete interior wide-band beam-column connections subjected to lateral earthquake loading." *ACI Struct. J.,* 98(3), 270-279.

Wong, H. F., and Kuang J. S. (2008). "Effects of beam-column depth ratio on joint seismic behaviour." *Proceedings of the Institution of Civil Engineers-Structures and Buildings* 161(2), 91-101.

Wosatko A, Pamin J, Polak MA., (2015), "Application of damage-plasticity models in finite element analysis of punching shear." *Comput Struct*, 151:73-85.